

PointVoxel: A Simple and Effective Pipeline for Multi-View Multi-Modal 3D Human Pose Estimation

Zhiyu Pan

Zhicheng Zhong

Wenxuan Guo

Yifan Chen

Jianjiang Feng*

Jie Zhou

Department of Automation, BNRist, Tsinghua University, China

{pzy20, zhongzc18, guowx22, chenyf21}@mails.tsinghua.edu.cn

{jjfeng, jzhou}@tsinghua.edu.cn

Abstract

Recently, several methods have been proposed to estimate 3D human pose from multi-view images and achieved impressive performance on public datasets collected in relatively easy scenarios. However, there are limited approaches for extracting 3D human skeletons from multi-modal inputs (e.g., RGB and pointcloud) that can enhance the accuracy of predicting 3D poses in challenging situations. We fill this gap by introducing a pipeline called PointVoxel that fuses multi-view RGB and pointcloud inputs to obtain 3D human poses. We demonstrate that volumetric representation is an effective architecture for integrating these different modalities. Moreover, in order to overcome the challenges of annotating 3D human pose labels in difficult scenarios, we develop a synthetic dataset generator for pretraining and design an unsupervised domain adaptation strategy so that we can obtain a well-trained 3D human pose estimator without using any manual annotations. We evaluate our approach on four datasets (two public datasets, one synthetic dataset, and one challenging dataset named BasketBall collected by ourselves), showing promising results. The code and dataset will be released soon.

1. Introduction

Human pose estimation is a fundamental task in computer vision and has been widely applied in various fields, such as human-computer interaction, human-robot interaction, human activity recognition, etc. Specifically, multi-view image datasets [4, 22, 25, 50] allow more precise 3D human pose estimation compared to single-view ones [1, 24, 34, 55], due to the ability of multiple views to capture 3D information from epipolar geometry. As technology advances, researchers [23, 33, 43, 48, 54] have achieved promising results on these multi-view images datasets. However, prac-

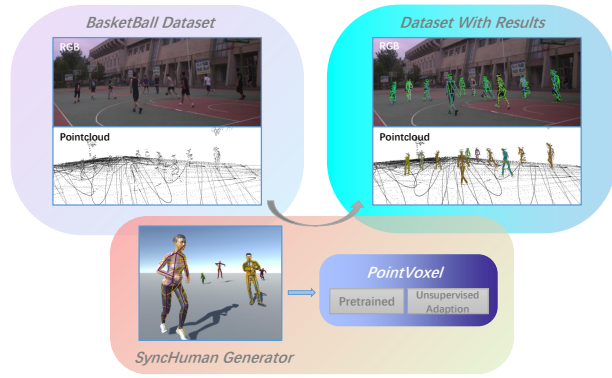


Figure 1. The overview of training a 3D human pose estimation network without using manual annotations. First, PointVoxel is pretrained on synthetic data generated by SyncHuman, and then unsupervisedly trained to adapt to the target dataset. The top row shows estimated human poses on a new dataset, BasketBall, which is collected by four camera-LiDAR sensors (only one RGB view is shown). The bottom row shows our synthetic dataset.

tical scenarios are more challenging than existing public datasets, with diverse human motions, severe occlusions, and large scene.

Combining different sensors such as LiDAR and RGB camera has the potential of boosting the accuracy of 3D human pose estimation performance in multiple situations. LiDAR sensor can obtain precise but quite sparse 3D measurements over long range, while camera can capture images of high resolution but lacks depth perception. Therefore, LiDAR-Camera capturing system can provide texture and depth information simultaneously in a large covering range. It makes it possible to capture complex human activities within a large scene such as basketball games with a small number of sensors, beneficial for system setup and reducing cost. Therefore, it is essential to consider integrating the information from sensors of various types and views, and fusing them into a cohesive representation which can significantly facilitate the accuracy of 3D human pose

*Corresponding author

estimation.

In this paper, we propose PointVoxel, a 3D human pose estimation pipeline taking multi-view multi-modal inputs. Volumetric representation is an effective and reasonable architecture to fuse RGB and pointcloud. Researchers [23, 43, 48, 53] have shown the effectiveness of voxel-based method. Voxel-based architecture can naturally model a space’s geometric characteristics. Besides, it is straightforward to either map the pointcloud information or back-project the 2D information into the 3D volumetric representation. Nevertheless, voxel-based method is not satisfactory for detecting pedestrians especially in large scene due to the large computational cost while defining volumetric space on it. Some pointcloud-based methods [30, 35, 42] illustrates that they can detect objects accurately with the assist of pointcloud. As to multi-modal features fusion [15, 19], we refer to the work BEVFusion [35] and unify different modalities into a volumetric space that reserve each modality’s geometric characteristics. Hence, PointVoxel combines human detection and voxel-based 3D human pose estimation in a top-down manner.

Manually annotating or capturing 3D poses for multiple individuals in large scenes is challenging, expensive, and hard to ensure generalizability to new scenarios. To achieve better results on challenging scenarios without pose labels, we adopt the approach of pretraining on a synthetic dataset first and then unsupervised domain adaption training on the target dataset. We develop a synthetic dataset generator named SyncHuman for generating pretrained data. It can generate a large amount of synthetic data with multi-modal information, and we can change LiDARs’ and cameras’ properties in the scene to meet practical needs. Furthermore, the actions of avatars are diverse, as they can be obtained from existing action files or pose annotation files sourced from public motion capture datasets like AMASS [38]. Accordingly, the synthetic data has accurate 3D pose groundtruth for a group of people with complex actions.

To overcome the disparity between synthetic data and real-world scenarios and achieve unsupervised domain adaption training, we propose an efficient strategy including entropy-selected pseudo 3D pose supervision, pseudo 2D pose supervision, and human pose prior constraints. Benefiting from volumetric representation, we can get the interpretable outputs’ form: 3D human joints’ heatmap. Heatmap represents a probability distribution, and we can calculate the information entropy of each heatmap channel to get the confidence of corresponding joint. It is an essential indicator for identifying the quality of predicted poses. Experiments show that entropy value is inverse proportional to the rationality of predicted poses. Hence, we can use the entropy to filter out unreasonable poses and get the pseudo 3D pose labels while unsupervised domain adaption training. Off-the-shelf 2D pose estimation meth-

ods [6, 12, 47, 52] are so robust that we can use them to generate the pseudo 2D pose labels. Moreover, we design an intuitive human prior loss for guaranteeing the rationality of adapted predicted 3D poses. According to the aforementioned schemes, we are able to construct a 3D human pose estimation algorithm based on multi-modal and multi-view data without the need for annotations on target dataset (Figure 2).

We summarize the contributions of this paper as follows:

- We proposed a simple and effective pipeline named PointVoxel to fuse multi-view multi-modal inputs and estimate multiple person 3D pose, and it achieves promising results on different datasets with different settings.
- We proposed a training strategy without using manual annotations that involves pretraining on synthetic data generated by SyncHuman and unsupervised domain adaption training on a target dataset.

2. Related Works

In this section, we conduct the literature review according to the two contribution points we proposed.

2.1. 3D Human Pose Estimation

Image-based. Basic 3D pose estimation method is in two stage that estimates the 2D pose first and then lifts it into 3D space [9, 23, 33, 43, 48, 51]. As to multi-person setting, some methods [9, 33] match pedestrians from different views and then locate them through 2D pose similarity. But they are not robust to inaccurate 2D pose results. Zhang et al. [54] directly utilizes the 2D images as inputs and regresses the 3D pose by transformer architecture. However, their training process is time-consuming. Some voxel-based methods [43, 48] locate each person in a 3D volumetric space and estimate 3D poses. Such voxel-based methods greatly improve the precision of 3D human pose estimation. However, they are not suitable for the large scene because of large computational cost when detecting people.

Pointcloud-based. In the beginning, there are some 3D pose estimation methods based on single-view depth map [13, 18, 20, 39]. They treat the depth map as 2D information with depth value. On the other hand, a few of methods back-project depth map into 3D space as dense 3D pointcloud and use Pointnet network to deal with [3, 57]. Moon et al. [40] propose a single-person pose estimation approach which treats depth map as pointcloud and fill it in volumetric space. Bekhtaoui et al. [3] use Pointnet related approach to detect and estimate 3D human pose. Recently, Li et al. [31] use sparse pointcloud scanned from LiDAR to estimate single-person 3D human pose. However, sparse pointcloud cannot provide enough information for accurate 3D pose estimation. Multi-modal fusion is helpful for concise 3D human poses’ perceiving.

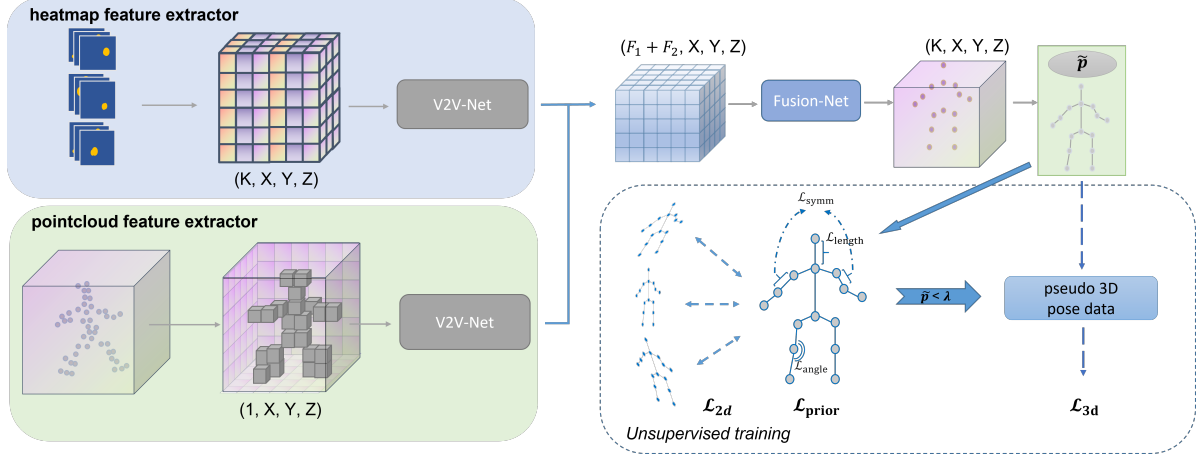


Figure 2. The detailed structure of PointVoxel in 3D human pose estimation and its unsupervised training strategy. Dashed arrows indicate calculating corresponding loss. \Rightarrow represents conditional flow which means the pose will be the pseudo 3D label for the next epoch if required condition is met.

Table 1. Comparison of the synthetic datasets about human beings.

Synthetic Dataset	Scene setup					Labels	
	Multi-View	Multi-Person	RGB Image	Depth Image	LiDAR Pointcloud	2D Pose	3D Pose
CAPE [37]	✗	✗	✗	✗	✗	✗	✓
SURREAL [49]	✗	✗	✓	✓	✗	✓	✓
PSP [11]	✗	✗	✓	✗	✗	✓	✗
CALAR [10]	✓	✓	✓	✓	✓	✗	✗
<i>Ours</i>	✓	✓	✓	✓	✓	✓	✓

Multi-modal based. Many works have been introduced for RGBD human pose estimation [2, 15, 19, 58]. Multi-modal information can not only help detect the person but also guarantee the accuracy of 3D human pose. Lately, some researchers [7, 31] introduce camera-LiDAR setting datasets for outdoors and large scene. As to the multi-modal fusion methods, some approaches [3, 19, 58] fuse modalities in point-level by attaching extracted 2D features to every 3D point. And a few methods [32, 41] fuse modalities in feature-level strategy. They do not unify the 2D and 3D information in a unified interpretable space, and fuse them in an uninterpretable feature space instead.

Our approach utilizes multi-modal information for human detection and 3D human pose estimation. Besides, we use volumetric representation representing real-word space to unify the 2D and 3D information.

2.2. Synthetic Dataset Generation

Manually annotating 3D human pose is very tough. Therefore, synthetic dataset is beneficial and helpful for pretraining model. There are many synthetic datasets for 3D human pose estimation [11, 37, 49]. However, these datasets are just single RGB view with random background. Besides, they do not consider the rational interaction between

avatars and the background. Dosovitskiy et al. [10] provides a large-scale synthetic dataset for autonomous driving. However, it dose not provide the 3D human pose labels, and the actions of characters are monotonous.

We propose our synthetic dataset generator SyncHuman which can produce data with more richness and diversity (Table 1). Moreover, we will publish the generating tool so that researchers can change settings according to their needs via our provided APIs.

2.3. Unsupervised Domain Adaption Training

There are many works in unsupervised or domain adaption manner for single view 3D human pose estimation. Kocabas et al. [27] use multi-view geometry to supervise single view’s predicting results. Several methods [28, 46] use teacher-student framework to conduct domain adaption. And a portion of approaches [8, 56] utilize optical-flow or depth as their inputs which are least affected by domain shift compared with RGB. Bigalke et al. [5] add human prior loss according to human anatomy. Kundu et al. [29] define the uncertainty of predictions and control the uncertainty value while training. For multi-view 3D human pose generation method, there are some works use non-deeplearning methods [4, 44]. 3DPS [4] and basic triangulation get 3D poses within large computing complexity or inaccuracy. Remelli et al. [44] proposed an efficient DLT (direct linear transformation) which can get relatively accurate 3D results quickly.

Our work uses different views 2D pose heatmaps and depths as inputs that are little influenced when changing domain. Besides, we choose information entropy as the network’s uncertainty index without any extra loss while training. Entropy can be used to select reliable results as pseudo 3D labels. Also, we add the human prior loss to ensure the

reasonability of 3D poses.

3. Methodology

The proposed method is composed of two parts: 3D human pose estimation and unsupervised domain adaption training (Figure 2). Section 3.1 introduces the approach of the top-down manner of 3D human pose estimation. We introduce the details about voxel-based multi-modal fusion. Section 3.2 illustrates how we generate the synthetic dataset to support the training of multi-modal pose estimation model, and how to combine entropy with the human prior loss to realize domain shift.

3.1. PointVoxel

Similar to [9, 43, 48], we adopt the top-down manner to estimate the 3D pose. In our case, we adopt PointPillars [30] to detect the 3D bounding box of each person. After obtaining the bounding box of each person, we can get the 2D bounding box in each view for 2D pose estimation, and extract their pointcloud. At first, we can define a volumetric space centered at the pointcloud’s centroid whose size is consistent with detected bounding boxes’, and discretize it into an $X \times Y \times Z$ resolution. So that we can fill each voxel according to each pointcloud’s coordinate. In our case, we set value 1 to the voxel containing pointcloud. Then we can get the pointcloud-related feature ($F_1 \times X \times Y \times Z$) via 3D convolution backbone V2V-Net [40].

Thanks to the development of 2D pose estimation methods [12, 52], relatively accurate corresponding 2D pose can be predicted without extra training. Hence, we can get each view’s 2D pose heatmap via Gaussian blur. We apply the same projecting way as [48] to calculate each voxel’s information, and apply V2V-Net to extract the rgb-related features ($F_2 \times X \times Y \times Z$) in 3D space. Then, we concatenate the two modal features in the same 3D space for modality fusion and get the final 3D human pose heatmap via a 3D convolution head Fusion-Net. In order to mitigate quantization error, we adopt *Soft-argmax* to calculate each joints’ 3D coordinate J^k through 3D heatmaps and minimize the L_1 loss with the ground truth J_*^k :

$$\mathcal{L}_{\text{pose}} = \sum_{k=1}^K \|J^k - J_*^k\|_1 \quad (1)$$

where K is the number of joints.

3.2. Unsupervised Domain Adaptation

Due to the lack of annotated multi-view multi-modal 3D human pose dataset, we choose to generate a synthetic dataset to assist training. SyncHuman we designed can create 3D dynamic scenes of multiple persons with accurate labels. Besides, we develop an efficient unsupervised domain adap-

tion means by designing a loss function to transfer the pre-trained model from synthetic dataset to real-world dataset.

3.2.1 SyncHuman Dataset

We develop the synthetic system based on Unity Engine. Due to its flexibility and productivity, we can formulate a scene with a specific size and background as per our specifications. Concerning sensors’ aspect, we implement Unity’s built-in camera to obtain RGB images, and extract the depth information from the GPU’s depth buffer with custom shaders used in the rendering pipeline. Furthermore, we can attain the colored pointcloud by sampling the depth and RGB images. For the sake of imitating the scanning process of LiDAR, we need to sample points along to a scanning function of time. Currently, we consider Livox Mid-40 LiDAR only, since its price is sufficiently low for sports or surveillance applications. We use the following function to simulate its scanning process:

$$r = \alpha \times \cos(3.825 \times (\theta_0 + 0.0017 \times n)) \quad (2)$$

where $n \in [0, t \times 1e5]$ and t is in second. α is the scanning radius in pixel, and θ_0 is a random initial angle. This equation is defined in polar coordinate. Final sampling points can be acquired by transforming it from polar coordinates to Cartesian coordinates and translating it to the center of the image space.

As for the avatars, we download various human 3D models from Adobe Mixamo¹. With a view to guarantee the diversity of the generated actions, we can drive these avatars by either ready-made action files or other public datasets’ keypoint annotations. Currently, we have developed the driving APIs for COCO17, COCO19 [34] and SMPL [36] standard keypoint annotated inputs. Regarding the groundtruth matter, we can obtain the 3D human pose from the avatars’ humanoid skeleton; 2D pose label can be acquired via projecting 3D pose into 2D view. Additionally, we can fetch the mesh vertex of each avatar and then compute the semantic segmentation label for each pointcloud by considering the pose label meanwhile.

3.2.2 Unsupervised Domain Adaptation

Similar to the 2D projection supervision utilized by other unsupervised or weakly supervised methods [16, 27], we directly employ off-the-shelf 2D human pose estimation model to get the pseudo 2D pose label \tilde{J}_{2D} . \mathcal{L}_{2D} is obtained by calculating the L_2 norm between 3D pose projection results and pseudo 2D label from each view.

$$\mathcal{L}_{2D} = \sum_{v=1}^V \sum_{k=1}^K \left\| \mathcal{P}_v(J^{v,k}) - \tilde{J}_{2D}^{v,k} \right\|_2 \quad (3)$$

¹<https://mixamo.com>

where \mathcal{P} is the projection function. V is the number of views. \mathcal{L}_{2D} is the fundamental loss for unsupervised training. In order to attain pseudo 3D label, we choose to use information entropy as one uncertainty index. The entropy of one keypoint prediction heatmap (a spatial probability distribution) h^k is defined as:

$$\mathcal{H}(h^k) = - \sum_i h_i^k \times \log h_i^k \quad (4)$$

where i represents the voxel index. The higher the entropy is, the more uncertain the keypoint location is. Furthermore, it relates to the rationality of the keypoint location as observed in our experiments (Section 4.5). To measure a person's uncertainty, we take the maximum entropy value of all keypoints. Different from Kundu et al. [29] who train the uncertainty value, we consider it as an inartificial index. Our experiments demonstrate that the magnitude of entropy values can serve as an indicator of pose estimation quality for a specific network. Therefore, an entropy threshold λ can be set to sort out the reasonable predicted 3D human poses. In other words, we select the predicted pose \tilde{p} whose entropy value is less than λ as the pseudo 3D pose label for the next epoch's training, and it can be updated after each training epoch. Therefore, the 3D pseudo pose loss can be obtained by:

$$\mathcal{L}_{3D} = \sum_{k=1}^K \left\| J^k - \tilde{J}^k \right\|_1 \quad (5)$$

where \tilde{J}^k is the 3D joint of the selected pseudo 3D pose label \tilde{p} .

To further ensure the anatomical plausibility of the pose, we introduce a human prior loss \mathcal{L}_{prior} ² adapted from Bigalke et al. [5]. Specifically, we formulate three losses to penalize asymmetric limb lengths \mathcal{L}_{symm} , implausible joint angles \mathcal{L}_{angle} , and implausible bone lengths \mathcal{L}_{length} . To sum up, the final loss function is defined as:

$$\mathcal{L}_{unsup} = \omega_1 \mathcal{L}_{2D} + \omega_2 \mathbb{1}(\tilde{p} < \lambda) \mathcal{L}_{3D} + \omega_3 \mathcal{L}_{prior} \quad (6)$$

where ω_1 , ω_2 and ω_3 are the weights of each loss.

4. Experiments

In this section, we introduce all datasets and evaluation metrics used in our experiments. We analyze the performance of our PointVoxel pipeline in supervised and unsupervised manner on different datasets. Besides, we also conduct ablation studies to verify the effectiveness of each strategy or loss in unsupervised domain adaption.

4.1. Implementation details.

We use V2V-Net [40] as the pointcloud and heatmap voxel's feature extractor. The detailed V2Vnet design is the same

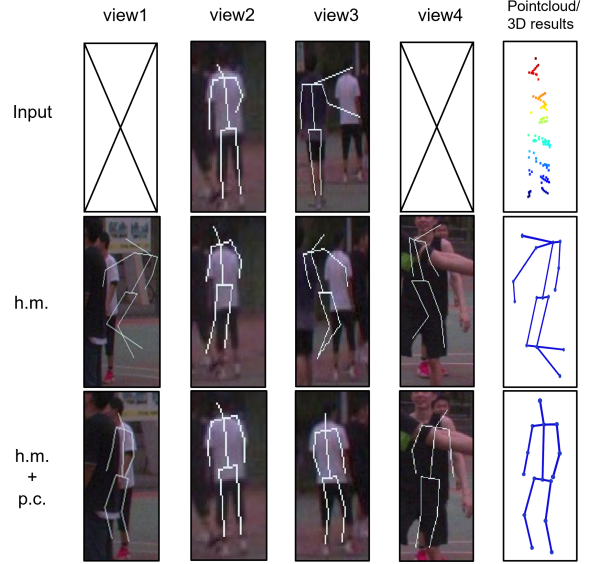


Figure 3. The results are from different inputs' modalities training on BasketBall. The first row is the 2D pose and pointcloud for model inputs, the second row's results are from the model trained by 2D pose heatmap (h.m.) inputs, and the third row's results are from the model trained by 2D pose heatmap and pointcloud (h.m.+p.c.) inputs. The pose results shown on image are from projected 3D ones except for the first row. Both models utilize the complete unsupervised training strategy.

with PRN [48]. The resolution of the voxel grid is $64 \times 64 \times 64$ defined in a $2m \times 2m \times 2m$ space. We set $\omega_1 = 0.02$, $\omega_2 = 1$, $\omega_3 = 10$, and $\lambda = 6$. We train the voxel-based pose estimation network on an NVIDIA GeForce RTX-3090 (24G) with a batch size of eight. The learning rate is set to 0.001 and the optimizer is Adam [26].

4.2. Datasets and Metrics.

We use the following datasets in our experiments:

I. CMU Panoptic Studio [25]. It is indoors with a valid scene range around $5m \times 5m$. In order to realize the multi-modal inputs, we select several subsets³ that were evaluated in [33] and have depth information. We unify the depth information from Kinect 1 to 5 and process these depth maps by equation 2 to get the sparse pointcloud which is similar to Mid-40 Livox LiDAR's scanning. About the 2D pose estimation results, we use the results provided by [33] which are claimed to be predicted from HRNet [47].

II. MVOR [45]. It is indoors set in operating room. In this dataset, we adopt three sampling functions (equation 2) centered at three trisection points of image's width to imitate a Mid-100 Livox LiDAR's scanning. And we use the

³“160422_ultimatum1”, “160224_haggling1”, “160226_haggling1”, “161202_haggling1”, “160906_ian1”, “160906_ian2”, “160906_ian3”, and “160906_band1” for training; “160906_pizza1”, “160422_haggling1”, “160906_ian5”, “160906_band2” for testing.

²Please refer to Suppl. for details.

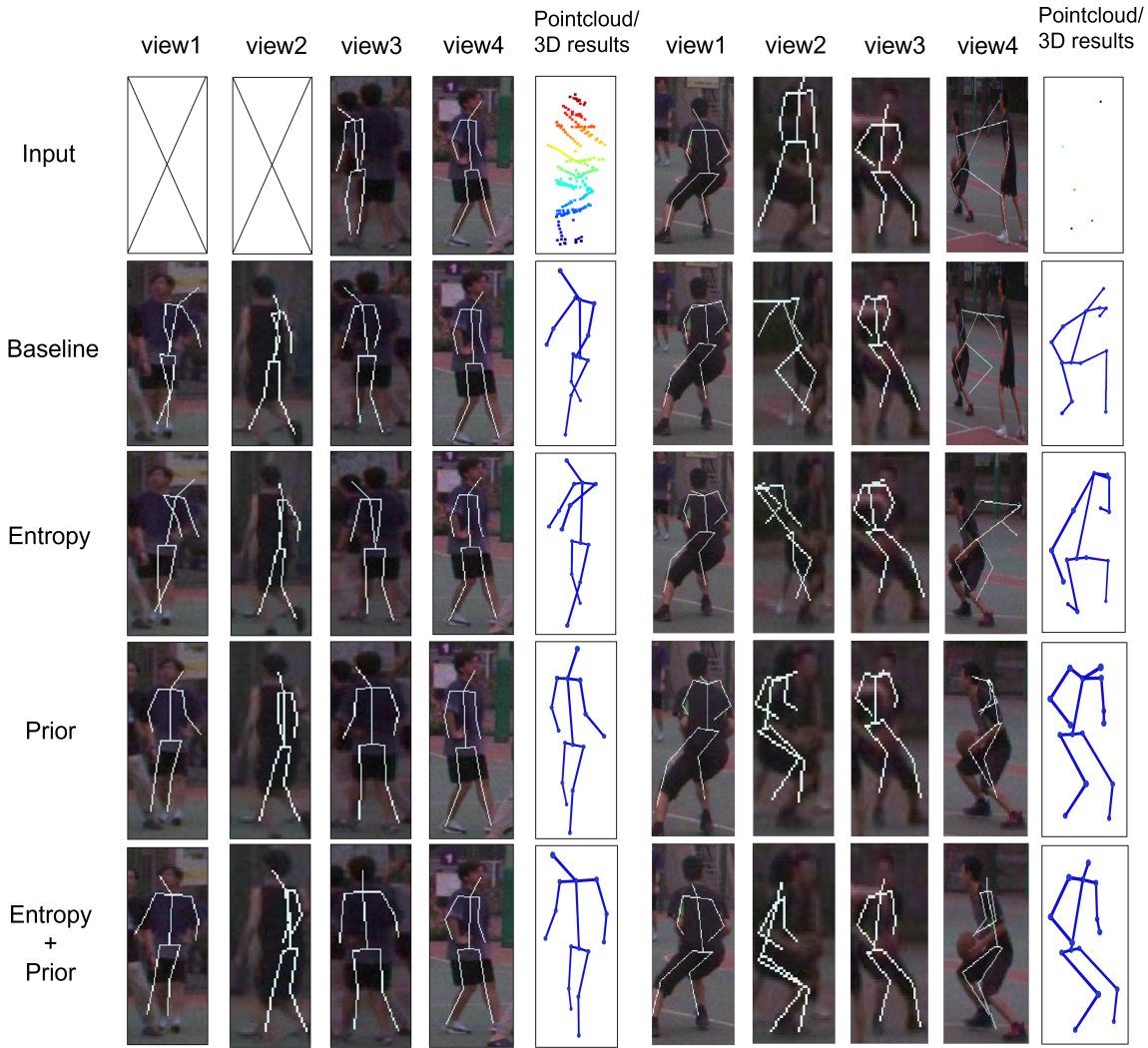


Figure 4. The results show the ablation study about unsupervised training losses on BasketBall. Baseline is only pseudo 2D pose supervision. “Entropy” means adding entropy-selected pseudo 3D pose supervision. “Prior” means adding human prior loss.

2D pose estimation results provided by [45] which are predicted from AlphaPose [12]. There is a semantic keypoints’ definition gap between MVOR (a ten keypoints standard) and ours (COCO17 standard). Therefore, we only conduct the qualitative analysis on MVOR. We use the data with annotation from “day1, day2, day3” for training and “day4” for testing.

III. Basketball. It is outdoors with a valid scene range around $35m \times 17m$ recording a basketball match. We collected this real-world dataset with four-view multi-modal information recording a basketball match. The pointcloud is collected by four Mid-100 Livox LiDARs. The 2D pose estimation results are predicted by VitPose [52]. The dataset contains two segments, each containing of two thousand frames. It has manually marked the detection and tracking groundtruth for each frame, while lacks of the 3D key-

points groundtruth. Therefore, it is mainly used for qualitative analysis.

IV. BasketballSync. It is a synthetic dataset generated by SyncHuman with the same sensors’ configuration and setting as Basketball. The pointcloud is obtained by simulating the scan pattern of Mid-100 Livox LiDARs. It contains ten avatars acting randomly with the first eight for training and the rest two for testing among all frames (3336 frames in 10Hz). The predicted 2D human poses are extracted by VitPose [52].

Evaluation metrics. For evaluating the 3D human pose, we calculate the standard mean per-joint position error before and after Procrustes Alignment [17] as MPJPE and PA-MPJPE in millimeter respectively. And we compare to the methods with single-frame data input like ours for fairness.

Table 2. Comparison of different 3D pose estimation methods on Panoptic and BasketBallSync. As to unsupervised manner, we pre-trained PointVoxel on BasketBallSync in Panoptic testing and on Panoptic in BasketBallSync testing.

Methods	Supervision	Panoptic		BasketBallSync	
		MPJPE	PA-MPJPE	MPJPE	PA-MPJPE
MvP [54]	sup.	25.78	25.02	291.11	240.32
PlanePose [33]	sup.	18.54	11.92	119.55	65.80
VoxelPose(PRN) [48]	sup.	14.91	11.88	40.80	34.34
<i>Ours</i>	sup.	14.44	11.61	31.84	27.36
DLT [44]	no sup.	38.26	44.77	101.49	62.77
<i>Ours</i>	no sup.	22.00	15.96	72.92	62.72

Table 3. Comparison of different input modalities for PointVoxel on Panoptic and BasketBallSync. Model tested on BasketBallSync is pretrained on Panoptic, and is pretrained on BasketBallSync for Panoptic testing.

Input modality	supervision	Panoptic		BasketBallSync	
		MPJPE	PA-MPJPE	MPJPE	PA-MPJPE
p.c.	sup.	164.30	148.78	136.01	123.22
h.m.	sup.	14.91	11.88	40.80	34.34
h.m.+p.c.	sup.	14.44	11.61	31.84	27.36
h.m.	no sup.	25.72	17.24	263.05	183.85
h.m.+p.c.	no sup.	22.00	15.96	72.92	62.72

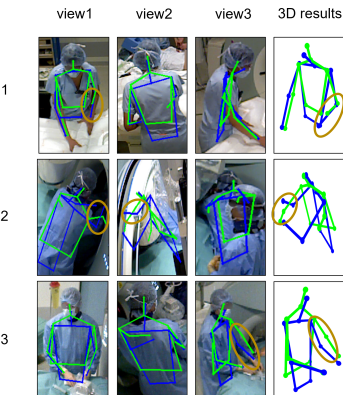


Figure 5. Qualitative results of 3D human pose estimation on MVOR from three samples. Blue lines represent the predictions and green lines represent the groundtruth. The first to third columns are the projected 2D results on three views and the fourth one is the 3D pose result.

4.3. 3D Pose Estimation Analysis

In this section, we evaluate the 3D human pose estimation results of different approaches. For PlaneSweepPose [33], VoxelPose [48] and PointVoxel in supervised manner, we utilize the groundtruth location of each person into the process of training and testing. As to MvP [54], it is difficult to add the groundtruth detection information into the network due to its architecture design, which also means that it cannot utilize the depth or pointcloud information directly.

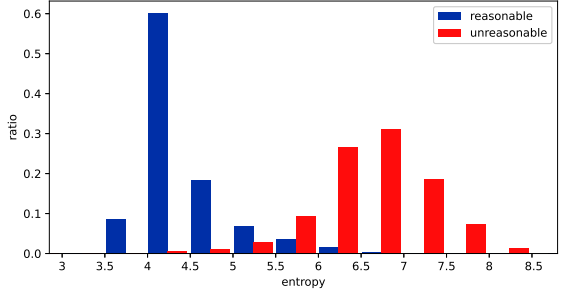


Figure 6. The entropy distributions of reasonable and unreasonable predicted 3D poses.

rectly. For fairness, we just evaluate the MPJPE@500 metrics (only considering per joint error less than 500 mm) for the matched person as to MvP.

We evaluate these approaches on Panoptic Studio and BasketballSync as small scene and large scene respectively. Table 2 shows that our approach outperforms them in terms of MPJPE and PA-MPJPE especially in large scene's setting. It is worth noting that our approach with unsupervised learning manner can even outperform supervised RGB inputs multi-view approaches.

We assess our pipeline on MVOR, and our method in unsupervised manner achieved great performance which even outperforms groundtruth in some frames (Figure 5).

Additionally, we analyze the performance with different modal inputs (pointcloud, RGB, and both of them) in volumetric architecture. Table 3 illustrates that the Livox pointcloud information alone is unable to accurately extract 3D human skeleton due to its sparsity, and cannot be adopted in unsupervised manner without 2D pseudo labels from heatmaps. However, when combined with RGB information, the performance is greatly enhanced. Figure 3 demonstrates that multi-modal inputs increase the model's tolerance to 2D pose estimation error, including severe situations like miss-prediction or predicting on a wrong person, during unsupervised domain adaption training.

4.4. Unsupervised Domain Adaption

In this section, we conduct an in-depth analysis of the settings of synthetic datasets and ablation studies of unsupervised training strategy.

4.4.1 Synthetic Setting

Tu et al. [48] have conducted an experiment by training VoxelPose with target dataset's camera configuration and others' human pose, then directly applying the model to target dataset for evaluation. In this section, we further analyze the impact of scene settings in volumetric architecture. We simulated four different scene setups by SyncHuman generator which changes the sensors' position and orientation.

Table 4. Comparison of different scene setups. We simulated four different scene setups by SyncHuman generator. This table shows the performance of PointVoxel by pretraining on different scenes and directly applying to Panoptic. “others.” means corresponding attribute is a setting that is different from Panoptic or BasketBall. “Pan.” means corresponding attribute is the same with Panoptic. “Bas.” means corresponding attribute is same with BasketBall.

Scene’s Range	Sensors’ Setting			Metric	
	Number	Position	Orientation	MPJPE	PA-MPJPE
Bas.	4	Bas.	Bas.	82.61	93.41
Bas.	5	others	Pan.	77.90	60.42
Pan.	5	others	Pan.	26.45	22.56
Pan.	5	Pan.	Pan.	23.15	17.63

Table 5. Comparison of different unsupervised training strategies. The model is pretrained on BasketBallSync for Panoptic testing, and on Panoptic for BasketBallSync testing. “Entropy” means adding entropy selected pseudo 3D pose supervision, and “Prior” means adding human prior loss.

Unsup. loss		Panoptic		BasketBallSync	
Entropy	Prior	MPJPE	PA-MPJPE	MPJPE	PA-MPJPE
✗	✗	29.14	16.48	84.49	75.55
✓	✗	28.26	25.85	77.38	68.84
✗	✓	22.88	24.69	76.45	65.54
✓	✓	22.00	15.96	72.92	62.72

Table 4 demonstrates that the more similar scene setups are, the better the model performs. It also suggests that in practical applications, setting the synthetic data to have the same sensor arrangement and scene range as the target dataset can improve the performance of unsupervised domain adaption or direct inferring on the new scenario.

4.4.2 Ablation Study on Unsupervised Training Losses

For unsupervised domain adaption, pseudo 2D pose supervision is necessary, and it is the baseline. Besides, we adopt an interpretable human prior loss and a pseudo 3D pose (selected by entropy value) loss to assist the learning. Therefore, we conduct an ablation study to analyze the impact of these two losses. From Table 5, entropy selected pseudo 3D pose loss improves the performance, but it does not limit the rationality which means it may generate low-entropy invalid 3D poses. Prior loss controls the results in reasonable action range. Therefore, we choose both losses as our efficient training strategy. Besides, these losses can enhance the robustness to 2D pose estimation errors (Figure 4).

4.5. Entropy Analysis

In order to verify the relationship between entropy value and pose rationality, we labeled some 3D poses predicted by PointVoxel as reasonable or unreasonable. Figure 6 shows

the distribution of entropy value for reasonable and unreasonable poses. Poses can be divided naturally via an entropy threshold. Therefore, we can judge one model’s performance on one unlabeled dataset by its average entropy value. It is noteworthy that it cannot reduce the entropy value for a model without proper pretraining after unsupervised learning. Hence, entropy-based judgement is more applicable before unsupervised adaption.

5. Limitation

The PointVoxel pipeline performs well in both supervised or unsupervised manner. However, it still has some problems to be addressed. 1) The method does not consider temporal information. 2) The unsupervised adaption performance on single view dataset is not good. 3) It suffers from the view-variant effect especially after unsupervised training. 4) The synthetic dataset currently does not set complex background, and the real basketball dataset is relatively limited in size.

6. Conclusion

In this paper, we propose a pipeline called PointVoxel for 3D human pose estimation using multi-view multi-modal data. To train the model in unsupervised manner, we develop a synthetic generator SyncHuman and design an efficient unsupervised loss for domain adaption learning. We conduct extensive experiments on both synthetic and real-world datasets. We analyze the powerful learning ability of this pipeline for 3D human pose estimation. Besides, we study the impact of scene settings and unsupervised training losses. Furthermore, we investigate the inherent relationship between entropy value and pose plausibility. We believe that our approach can be a good baseline for large scene’s multi-view multi-modal 3D human pose estimation.

References

[1] Mykhaylo Andriluka, Leonid Pishchulin, Peter Gehler, and Bernt Schiele. 2D human pose estimation: New benchmark

and state of the art analysis. In *Proceedings of the IEEE Conference on Computer Vision and Pattern Recognition*, pages 3686–3693, 2014. 1

[2] Renat Bashirov, Anastasia Ianina, Karim Iskakov, Yevgeniy Kononenko, Valeriya Strizhkova, Victor Lempitsky, and Alexander Vakhitov. Real-time rgbd-based extended body pose estimation. In *Proceedings of the IEEE/CVF Winter Conference on Applications of Computer Vision*, pages 2807–2816, 2021. 3

[3] Walid Bekhtaoui, Ruhan Sa, Brian Teixeira, Vivek Singh, Klaus Kirchberg, Yao-jen Chang, and Ankur Kapoor. View invariant human body detection and pose estimation from multiple depth sensors. *arXiv preprint arXiv:2005.04258*, 2020. 2, 3

[4] Vasileios Belagiannis, Sikandar Amin, Mykhaylo Andriluka, Bernt Schiele, Nassir Navab, and Slobodan Ilic. 3D pictorial structures for multiple human pose estimation. In *Proceedings of the IEEE Conference on Computer Vision and Pattern Recognition*, pages 1669–1676, 2014. 1, 3

[5] Alexander Bigalke, Lasse Hansen, Jasper Diesel, and Matthias P Heinrich. Domain adaptation through anatomical constraints for 3D human pose estimation under the cover. In *International Conference on Medical Imaging with Deep Learning*, pages 173–187, 2022. 3, 5, 1

[6] Zhe Cao, Tomas Simon, Shih-En Wei, and Yaser Sheikh. Realtime multi-person 2D pose estimation using part affinity fields. In *Proceedings of the IEEE Conference on Computer Vision and Pattern Recognition*, pages 7291–7299, 2017. 2

[7] Peishan Cong, Yiteng Xu, Yiming Ren, Juze Zhang, Lan Xu, Jingya Wang, Jingyi Yu, and Yuexin Ma. Weakly supervised 3D multi-person pose estimation for large-scale scenes based on monocular camera and single LiDAR. *arXiv preprint arXiv:2211.16951*, 2022. 3

[8] Carl Doersch and Andrew Zisserman. Sim2real transfer learning for 3D human pose estimation: motion to the rescue. *Advances in Neural Information Processing Systems*, 32, 2019. 3

[9] Junting Dong, Wen Jiang, Qixing Huang, Hujun Bao, and Xiaowei Zhou. Fast and robust multi-person 3D pose estimation from multiple views. In *Proceedings of the IEEE/CVF Conference on Computer Vision and Pattern Recognition*, pages 7792–7801, 2019. 2, 4

[10] Alexey Dosovitskiy, German Ros, Felipe Codevilla, Antonio Lopez, and Vladlen Koltun. CARLA: An open urban driving simulator. In *Conference on Robot Learning*, pages 1–16, 2017. 3

[11] Salehe Erfanian Ebadi, You-Cyuan Jhang, Alex Zook, Saurav Dhakad, Adam Crespi, Pete Parisi, Steven Borkman, Jonathan Hogins, and Sujoy Ganguly. PeopleSansPeople: a synthetic data generator for human-centric computer vision. *arXiv preprint arXiv:2112.09290*, 2021. 3

[12] Hao-Shu Fang, Jiefeng Li, Hongyang Tang, Chao Xu, Haoyi Zhu, Yuliang Xiu, Yong-Lu Li, and Cewu Lu. Alpha-pose: Whole-body regional multi-person pose estimation and tracking in real-time. *IEEE Transactions on Pattern Analysis and Machine Intelligence*, 2022. 2, 4, 6

[13] Nicola Garau, Niccolò Bisagno, Piotr Bródka, and Nicola Conci. DECA: Deep viewpoint-equivariant human pose estimation using capsule autoencoders. In *Proceedings of the IEEE/CVF International Conference on Computer Vision*, pages 11677–11686, 2021. 2

[14] Andreas Geiger, Philip Lenz, and Raquel Urtasun. Are we ready for autonomous driving? the KITTI vision benchmark suite. In *Proceedings of the IEEE Conference on Computer Vision and Pattern Recognition*, pages 3354–3361, 2012. 2

[15] Beerend GA Gerats, Jelmer M Wolterink, and Ivo AMJ Broeders. 3D human pose estimation in multi-view operating room videos using differentiable camera projections. *Computer Methods in Biomechanics and Biomedical Engineering: Imaging & Visualization*, pages 1–9, 2022. 2, 3

[16] Mohsen Gholami, Ahmad Rezaei, Helge Rhodin, Rabab Ward, and Z Jane Wang. Self-supervised 3D human pose estimation from video. *Neurocomputing*, 488:97–106, 2022. 4

[17] John C Gower. Generalized procrustes analysis. *Psychometrika*, 40:33–51, 1975. 6

[18] Hengkai Guo, Guijin Wang, Xinghao Chen, and Cairong Zhang. Towards good practices for deep 3D hand pose estimation. *arXiv preprint arXiv:1707.07248*, 2017. 2

[19] Lasse Hansen, Marlin Siebert, Jasper Diesel, and Matthias P Heinrich. Fusing information from multiple 2D depth cameras for 3D human pose estimation in the operating room. *International Journal of Computer Assisted Radiology and Surgery*, 14:1871–1879, 2019. 2, 3

[20] Albert Haque, Boya Peng, Zelun Luo, Alexandre Alahi, Serena Yeung, and Li Fei-Fei. Towards viewpoint invariant 3D human pose estimation. In *Proceedings of the European Conference on Computer Vision*, pages 160–177, 2016. 2

[21] Yunzhong Hou, Liang Zheng, and Stephen Gould. Multi-view detection with feature perspective transformation. In *Proceedings of the European Conference on Computer Vision*, pages 1–18, 2020. 3

[22] Catalin Ionescu, Dragos Papava, Vlad Olaru, and Cristian Sminchisescu. Human3.6M: Large scale datasets and predictive methods for 3D human sensing in natural environments. *IEEE Transactions on Pattern Analysis and Machine Intelligence*, 36(7):1325–1339, 2013. 1

[23] Karim Iskakov, Egor Burkov, Victor Lempitsky, and Yury Malkov. Learnable triangulation of human pose. In *Proceedings of the IEEE/CVF International Conference on Computer Vision*, pages 7718–7727, 2019. 1, 2

[24] Sheng Jin, Lumin Xu, Jin Xu, Can Wang, Wentao Liu, Chen Qian, Wanli Ouyang, and Ping Luo. Whole-body human pose estimation in the wild. In *Proceedings of the European Conference on Computer Vision*, pages 196–214, 2020. 1

[25] Hanbyul Joo, Hao Liu, Lei Tan, Lin Gui, Bart Nabbe, Iain Matthews, Takeo Kanade, Shohei Nobuhara, and Yaser Sheikh. Panoptic studio: A massively multiview system for social motion capture. In *Proceedings of the IEEE International Conference on Computer Vision*, pages 3334–3342, 2015. 1, 5

[26] Diederik P Kingma and Jimmy Ba. Adam: A method for stochastic optimization. *arXiv preprint arXiv:1412.6980*, 2014. 5

[27] Muhammed Kocabas, Salih Karagoz, and Emre Akbas. Self-supervised learning of 3D human pose using multi-view

geometry. In *Proceedings of the IEEE/CVF Conference on Computer Vision and Pattern Recognition*, pages 1077–1086, 2019. 3, 4

[28] Jogendra Nath Kundu, Ambareesh Revanur, Govind Vitthal Waghmare, Rahul Mysore Venkatesh, and R Venkatesh Babu. Unsupervised cross-modal alignment for multi-person 3D pose estimation. In *Proceedings of the European Conference on Computer Vision*, pages 35–52, 2020. 3

[29] Jogendra Nath Kundu, Siddharth Seth, Pradyumna YM, Varun Jampani, Anirban Chakraborty, and R Venkatesh Babu. Uncertainty-aware adaptation for self-supervised 3D human pose estimation. In *Proceedings of the IEEE/CVF Conference on Computer Vision and Pattern Recognition*, pages 20448–20459, 2022. 3, 5

[30] Alex H Lang, Sourabh Vora, Holger Caesar, Lubing Zhou, Jiong Yang, and Oscar Beijbom. PointPillars: Fast encoders for object detection from point clouds. In *Proceedings of the IEEE/CVF Conference on Computer Vision and Pattern Recognition*, pages 12697–12705, 2019. 2, 4, 3

[31] Jialian Li, Jingyi Zhang, Zhiyong Wang, Siqi Shen, Chenglu Wen, Yuexin Ma, Lan Xu, Jingyi Yu, and Cheng Wang. Lidarcap: Long-range marker-less 3d human motion capture with lidar point clouds. In *Proceedings of the IEEE/CVF Conference on Computer Vision and Pattern Recognition*, pages 20502–20512, 2022. 2, 3

[32] Ming Liang, Bin Yang, Shenlong Wang, and Raquel Urtasun. Deep continuous fusion for multi-sensor 3D object detection. In *Proceedings of the European Conference on Computer Vision*, pages 641–656, 2018. 3

[33] Jiahao Lin and Gim Hee Lee. Multi-view multi-person 3D pose estimation with Plane Sweep Stereo. In *Proceedings of the IEEE/CVF Conference on Computer Vision and Pattern Recognition*, pages 11886–11895, 2021. 1, 2, 5, 7

[34] Tsung-Yi Lin, Michael Maire, Serge Belongie, James Hays, Pietro Perona, Deva Ramanan, Piotr Dollár, and C Lawrence Zitnick. Microsoft COCO: Common objects in context. In *Proceedings of the European Conference on Computer Vision*, pages 740–755, 2014. 1, 4

[35] Zhijian Liu, Haotian Tang, Alexander Amini, Xinyu Yang, Huizi Mao, Daniela Rus, and Song Han. BEVFusion: Multi-task multi-sensor fusion with unified bird’s-eye view representation. *arXiv preprint arXiv:2205.13542*, 2022. 2

[36] Matthew Loper, Naureen Mahmood, Javier Romero, Gerard Pons-Moll, and Michael J Black. SMPL: A skinned multi-person linear model. *ACM Transactions on Graphics*, 34(6):1–16, 2015. 4

[37] Qianli Ma, Jinlong Yang, Anurag Ranjan, Sergi Pujades, Gerard Pons-Moll, Siyu Tang, and Michael J Black. Learning to dress 3D people in generative clothing. In *Proceedings of the IEEE/CVF Conference on Computer Vision and Pattern Recognition*, pages 6469–6478, 2020. 3

[38] Naureen Mahmood, Nima Ghorbani, Nikolaus F Troje, Gerard Pons-Moll, and Michael J Black. AMASS: Archive of motion capture as surface shapes. In *Proceedings of the IEEE/CVF International Conference on Computer Vision*, pages 5442–5451, 2019. 2

[39] Angel Martínez-González, Michael Villamizar, Olivier Canévet, and Jean-Marc Odobez. Residual pose: A decoupled approach for depth-based 3D human pose estimation. In *IEEE/RSJ International Conference on Intelligent Robots and Systems*, pages 10313–10318, 2020. 2

[40] Gyeongsik Moon, Ju Yong Chang, and Kyoung Mu Lee. V2V-Posenet: Voxel-to-voxel prediction network for accurate 3D hand and human pose estimation from a single depth map. In *Proceedings of the IEEE conference on Computer Vision and Pattern Recognition*, pages 5079–5088, 2018. 2, 4, 5

[41] AJ Piergiovanni, Vincent Casser, Michael S Ryoo, and Anelia Angelova. 4D-net for learned multi-modal alignment. In *Proceedings of the IEEE/CVF International Conference on Computer Vision*, pages 15435–15445, 2021. 3

[42] Charles R Qi, Or Litany, Kaiming He, and Leonidas J Guibas. Deep hough voting for 3D object detection in point clouds. In *Proceedings of the IEEE/CVF International Conference on Computer Vision*, pages 9277–9286, 2019. 2

[43] N Dinesh Reddy, Laurent Guigues, Leonid Pishchulin, Jayan Eledath, and Srinivasa G Narasimhan. Tesseltrack: End-to-end learnable multi-person articulated 3D pose tracking. In *Proceedings of the IEEE/CVF Conference on Computer Vision and Pattern Recognition*, pages 15190–15200, 2021. 1, 2, 4

[44] Edoardo Remelli, Shangchen Han, Sina Honari, Pascal Fua, and Robert Wang. Lightweight multi-view 3D pose estimation through camera-disentangled representation. In *Proceedings of the IEEE/CVF Conference on Computer Vision and Pattern Recognition*, pages 6040–6049, 2020. 3, 7

[45] Vinkle Srivastav, Thibaut Issenhuth, Abdolrahim Kadkhodamohammadi, Michel de Mathelin, Afshin Gangi, and Nicolas Padoy. Mvor: A multi-view rgb-d operating room dataset for 2D and 3D human pose estimation. *arXiv preprint arXiv:1808.08180*, 2018. 5, 6

[46] Vinkle Srivastav, Afshin Gangi, and Nicolas Padoy. Self-supervision on unlabelled or data for multi-person 2D/3D human pose estimation. In *Medical Image Computing and Computer Assisted Intervention*, pages 761–771, 2020. 3

[47] Ke Sun, Bin Xiao, Dong Liu, and Jingdong Wang. Deep high-resolution representation learning for human pose estimation. In *Proceedings of the IEEE/CVF Conference on Computer Vision and Pattern Recognition*, pages 5693–5703, 2019. 2, 5

[48] Hanyue Tu, Chunyu Wang, and Wenjun Zeng. VoxelPose: Towards multi-camera 3D human pose estimation in wild environment. In *Proceedings of the European Conference on Computer Vision*, pages 197–212, 2020. 1, 2, 4, 5, 7, 3

[49] Gul Varol, Javier Romero, Xavier Martin, Naureen Mahmood, Michael J Black, Ivan Laptev, and Cordelia Schmid. Learning from synthetic humans. In *Proceedings of the IEEE Conference on computer vision and pattern recognition*, pages 109–117, 2017. 3

[50] Timo Von Marcard, Roberto Henschel, Michael J Black, Bodo Rosenhahn, and Gerard Pons-Moll. Recovering accurate 3D human pose in the wild using imus and a moving camera. In *Proceedings of the European Conference on Computer Vision*, pages 601–617, 2018. 1

[51] Size Wu, Sheng Jin, Wentao Liu, Lei Bai, Chen Qian, Dong Liu, and Wanli Ouyang. Graph-based 3D multi-person pose

estimation using multi-view images. In *Proceedings of the IEEE/CVF International Conference on Computer Vision*, pages 11148–11157, 2021. 2

[52] Yufei Xu, Jing Zhang, Qiming Zhang, and Dacheng Tao. Vitpose: Simple vision transformer baselines for human pose estimation. *arXiv preprint arXiv:2204.12484*, 2022. 2, 4, 6

[53] Hang Ye, Wentao Zhu, Chunyu Wang, Rujie Wu, and Yizhou Wang. Faster VoxelPose: Real-time 3d human pose estimation by orthographic projection. In *Proceedings of the European Conference on Computer Vision*, pages 142–159, 2022. 2

[54] Jianfeng Zhang, Yujun Cai, Shuicheng Yan, Jiashi Feng, et al. Direct multi-view multi-person 3D pose estimation. *Advances in Neural Information Processing Systems*, 34: 13153–13164, 2021. 1, 2, 7

[55] Song-Hai Zhang, Rui long Li, Xin Dong, Paul Rosin, Zixi Cai, Xi Han, Dingcheng Yang, Haozhi Huang, and Shi-Min Hu. Pose2seg: Detection free human instance segmentation. In *Proceedings of the IEEE/CVF Conference on Computer Vision and Pattern Recognition*, pages 889–898, 2019. 1

[56] Xiheng Zhang, Yongkang Wong, Mohan S Kankanhalli, and Weidong Geng. Unsupervised domain adaptation for 3D human pose estimation. In *Proceedings of the 27th ACM International Conference on Multimedia*, pages 926–934, 2019. 3

[57] Zihao Zhang, Lei Hu, Xiaoming Deng, and Shihong Xia. Sequential 3D human pose estimation using adaptive point cloud sampling strategy. In *International Joint Conferences on Artificial Intelligence Organization*, pages 1330–1337, 2021. 2

[58] Jingxiao Zheng, Xinwei Shi, Alexander Gorban, Junhua Mao, Yang Song, Charles R Qi, Ting Liu, Visesh Chari, Andre Cornman, Yin Zhou, et al. Multi-modal 3D human pose estimation with 2D weak supervision in autonomous driving. In *Proceedings of the IEEE/CVF Conference on Computer Vision and Pattern Recognition*, pages 4478–4487, 2022. 3

PointVoxel: A Simple and Effective Pipeline for Multi-View Multi-Modal 3D Human Pose Estimation

Supplementary Material

7. Different Scanning Patterns of Pointcloud

There are different ways to get or scan the pointcloud: 1) randomly sampling the depth map; 2) sampling the depth map with multiple equidistant horizontal lines to imitate Velodyne LiDARs; 3) sampling the depth map with the “Rose curve” sampling equation mentioned in our paper to imitate Livox LiDARs. Figure 7 shows that the “Rose curve” sampling equation provides minimal information due to its localized concentrated scan. However, Livox LiDARs are more affordable than Velodyne LiDARs, and they have been used in many applications including surveillance. Besides, our BaseketBall data is captured by Livox LiDARs. Therefore, we use the Livox scanning pattern to simulate scanning pointcloud in our experiments.

8. Datasets: BaseketBall and SyncHuman

8.1. BaseketBall

BasketBall is an outdoor dataset capturing a Basketball match with four sensor nodes (each node includes one Livox LiDAR and one RGB camera) in a convergent acquisition. The dataset is challenging due to large covering, occlusions, and players’ dynamic motions (Figure 8). Currently, we have developed an annotation tool to annotate the players’ 3D bounding boxes and IDs. In the future, we will integrate the 3D human keypoints annotation into the tool with the assist of PointVoxel.

8.2. SyncHuman

We can use our synthetic data generator SyncHuman to simulate any arrangement of sensors to observe a scene. As illustrated in Experiments of our paper, using the same scene setting for both training and test yields better transferring performance. Figure 8 shows the datasets we generated, PanopticSync and BaseketBallSync, compared with the original datasets.

9. Human Prior Loss

We use the human prior loss similar to [5] to encourage the network to generate human-like 3D keypoints. The human prior loss is defined as three parts: 1) the predicting bone length should be in a reasonable range; 2) the predicting length of symmetric bones should be similar; 3) the predicting bone angles should be reasonable according to the kinematic of human.

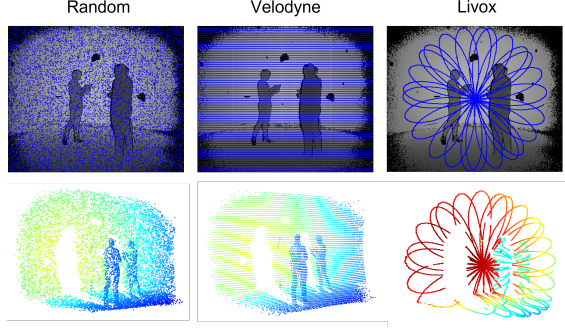


Figure 7. Different scanning patterns of pointcloud. All the samples shown in this figure are from the same scene at the same time, and contain the same number of points.

Different from Bigalke et al. [5] who distribute each joint with a specific length range, we set one range for all bones. In our case, we set $l_{\min} = 0.05\text{m}$ and $l_{\max} = 0.7\text{m}$. So the $\mathcal{L}_{\text{length}}$ can be defined as:

$$\mathcal{L}_{\text{length}} = \sum_{b=1}^N \mathcal{C}(B_i - l_{\max}, 0) + \mathcal{C}(l_{\min} - B_i, 0) \quad (7)$$

where $\mathcal{C}()$ is the clipping function that clip the value greater than 0, N is the number of bones. As to the symmetric bones, we set the symmetric bones as a pair, and set L_2 loss among them. So the $\mathcal{L}_{\text{symm}}$ can be defined as:

$$\mathcal{L}_{\text{symm}} = \sum_{b=1}^N \|B_i - B_{\text{symm}(i)}\|_2 \quad (8)$$

where B_{symm} is the symmetric bone of B_i . As to angle loss, we limit the nose-neck-midhip angle and hip-knee-ankle angle specifically to let nose be in front of the body and legs be bent forward. Figure 9 shows the definition of each joint and vectors. Specially, we do not directly calculate the angle of the bones, but calculate the dot product of corresponding vectors. First, we calculate the forward direction vector \vec{d}_{forward} of the body, which is the cross product of the unit vector from neck to midhip $\overrightarrow{J_0J_2}$ and unit vector from neck to left shoulder $\overrightarrow{J_0J_3}$:

$$\vec{d}_{\text{forward}} = \overrightarrow{J_0J_2} \times \overrightarrow{J_0J_3} \quad (9)$$

Then, as to the nose-neck-midhip angle, we calculate the unit vector from neck to nose $\overrightarrow{J_1J_0}$ denoted by \vec{d}_{nose} , and

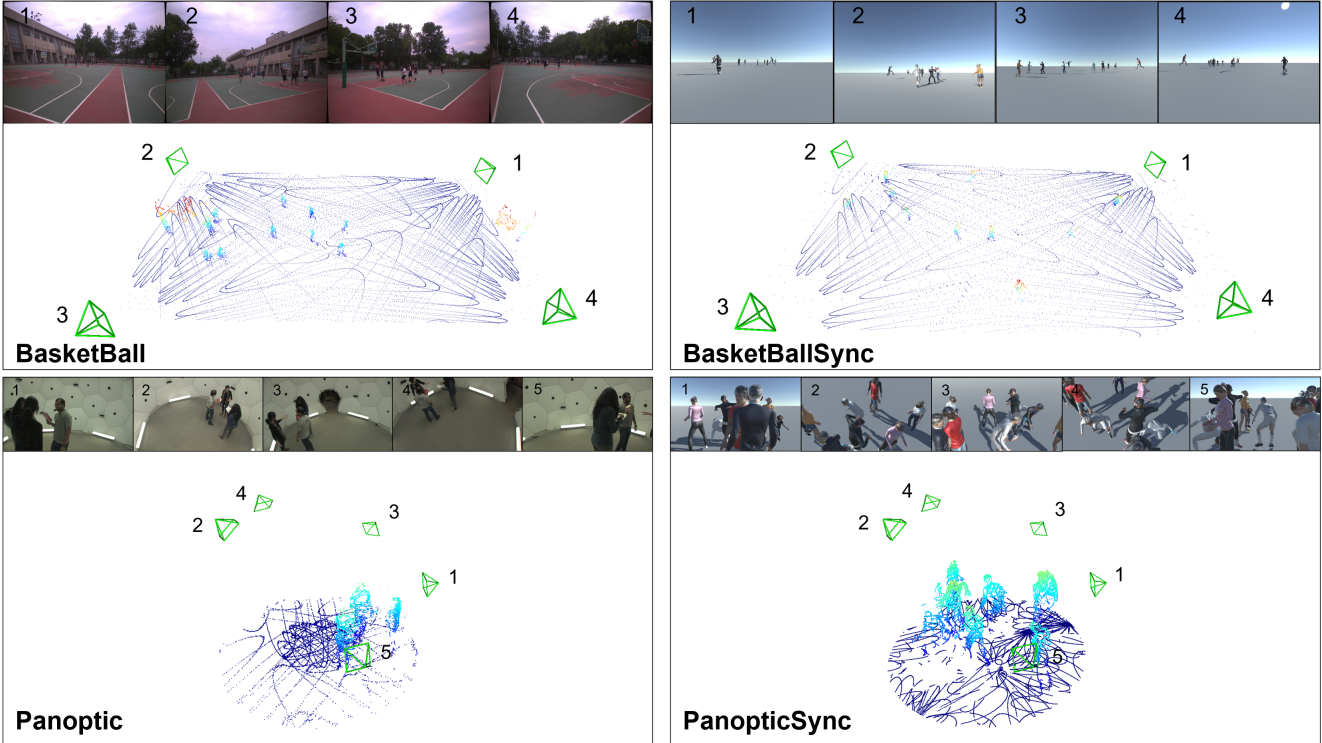


Figure 8. Real datasets and the synthetic datasets generated by SyncHuman.

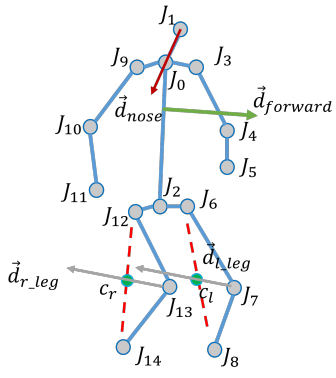


Figure 9. Definition of $\mathcal{L}_{\text{angle}}$.

we calculate the dot product of \vec{d}_{nose} and \vec{d}_{forward} and get the head angle loss:

$$\mathcal{L}_{\text{head_ang}} = \mathcal{C}(\vec{d}_{\text{forward}} \cdot \vec{d}_{\text{nose}}, 0, 1) \quad (10)$$

where $\mathcal{C}()$ is the clipping function that clip the value into 0 to 1. As to the hip-knee-ankle angle, we need to get the midpoint of the hip and ankle denoted by c_l and c_r for left leg and right leg respectively. Then, we calculate the unit vectors from knee point to the leg's midpoint as $\vec{d}_{l,\text{leg}}$ and

$\vec{d}_{\text{r-leg}}$. Therefore, we get the leg angle loss:

$$\mathcal{L}_{\text{leg_ang}} = \mathcal{C}(d_{\text{forward}} \cdot d_{\text{l_leg}}, 0, 1) + \mathcal{C}(d_{\text{forward}} \cdot d_{\text{r_leg}}, 0, 1) \quad (11)$$

where $\mathcal{C}()$ is the clipping function that clip the value into 0 to 1. Therefore, we can calculate the angle loss:

$$\mathcal{L}_{\text{angle}} = \mathcal{L}_{\text{head_ang}} + \mathcal{L}_{\text{leg_ang}} \quad (12)$$

Finally, we combine the three losses together as the human prior loss:

$$\mathcal{L}_{\text{prior}} = \gamma_1 \mathcal{L}_{\text{length}} + \gamma_2 \mathcal{L}_{\text{symm}} + \gamma_3 \mathcal{L}_{\text{angle}} \quad (13)$$

where γ_1 , γ_2 and γ_3 are the weights of each loss. In our case, we set all the weights as 1.

10. Extended Experiments

In this section, we conduct the experiments to verify the advantages of pointcloud input in pedestrian detection. Furthermore, we show more examples to explain the relationship between entropy value and pose rationality.

10.1. Human Detection

As for evaluating human detection, we assess the performance using the established average precision (AP) metric as described in KITTI [14]. And we regard detections as

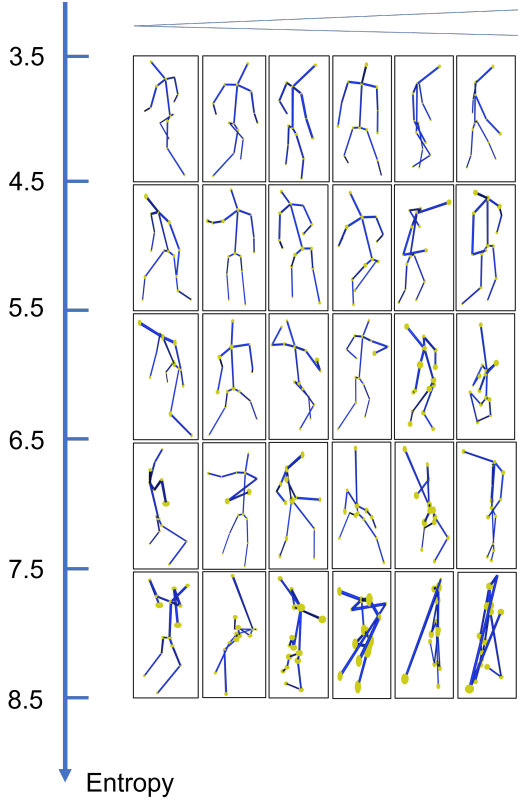


Figure 10. The entropy value and the specific poses. \swarrow represents an increasing entropy value from left to right among row’s samples. The size of joints’ ball represents the magnitude of the joint’s entropy value.

true positives to overlap by more than 70% (AP_{70}) or 50% (AP_{50}).

In the application of our current experiment, we adopt PointPillars [30] to detect the human bounding box. And we utilize the VoxelPose’s CPN [48] and MVDet [21] which is more suitable in large scene’s application as for comparison in terms of multi-view RGB-based methods. In CMU panoptic studio setup, VoxelPose [48] can get relatively accurate center location. However, it set the size of bounding box to be a constant value (We set $0.8m \times 0.8m \times 1.9m$ in our case for tighting results instead of $2m \times 2m \times 2m$ in [48]) which affects the performance of detection. In BasketBall, we adopt MVDet to detect human beings. Table 6 shows that pointcloud-based method outperforms the multi-view RGB-based method in terms of AP_{50} and AP_{70} benefiting from original poincloud’s 3D information. Besides, we verify the generalization ability of the pointcloud-based method by pretraining it on our synthetic dataset, and it still has an acceptable result.

Table 6. Human detection results on different datasets. “#” means using synthetic datasets (BasketBallSync and Panoptic-Sync) to pretrain and directly evaluate on corresponding real-world datasets.

Datasets	Methods	Metric	
		AP_{50}	AP_{70}
BasketBall	MVDet	69.41	37.66
	PointPillars#	88.17	44.26
	PointPillars	89.77	69.96
Panoptic	VoxelPose	21.17	0.19
	PointPillars#	40.17	6.25
	PointPillars	73.83	13.97

10.2. Entropy Analysis

Figure 10 shows the entropy value and the specific poses, and we can find that the 3D poses become more and more irrational while the entropy goes up.